

A METHOD FOR THE KINEMATICAL ANALYSIS OF  
LEED INTENSITY DATA

**RECEIVED**  
**LAWRENCE**  
**RADIATION LABORATORY**

SEP 11 1970

**LIBRARY AND**  
**DOCUMENTS SECTION**

R. Kaplan

July 1970

AEC Contract No. W-7405-eng-48

**TWO-WEEK LOAN COPY**

*This is a Library Circulating Copy  
which may be borrowed for two weeks.  
For a personal retention copy, call  
Tech. Info. Division, Ext. 5545*

**LAWRENCE RADIATION LABORATORY**  
**UNIVERSITY of CALIFORNIA BERKELEY**

## **DISCLAIMER**

This document was prepared as an account of work sponsored by the United States Government. While this document is believed to contain correct information, neither the United States Government nor any agency thereof, nor the Regents of the University of California, nor any of their employees, makes any warranty, express or implied, or assumes any legal responsibility for the accuracy, completeness, or usefulness of any information, apparatus, product, or process disclosed, or represents that its use would not infringe privately owned rights. Reference herein to any specific commercial product, process, or service by its trade name, trademark, manufacturer, or otherwise, does not necessarily constitute or imply its endorsement, recommendation, or favoring by the United States Government or any agency thereof, or the Regents of the University of California. The views and opinions of authors expressed herein do not necessarily state or reflect those of the United States Government or any agency thereof or the Regents of the University of California.

A METHOD FOR THE KINEMATICAL ANALYSIS OF  
LEED INTENSITY DATA

R. Kaplan\*

Inorganic Materials Research Division, Lawrence Radiation Laboratory  
and Department of Chemistry, University of California  
Berkeley, California 94720

ABSTRACT

A method is described for the kinematical analysis of intensity data in low-energy electron diffraction experiments. The method allows the plotting of intensity data for all diffraction beams and surfaces of a given crystal on a single graph, determining the crystal inner potential and the lattice parameter near the surface. Expressions are derived for application to seven surfaces of bcc and fcc crystals; extension to other surfaces and crystal structures is straightforward. The results are applied to intensity data for chromium and aluminum.

---

\* On sabbatical leave from the Naval Research Laboratory, Washington, D. C. 20390.

## I. INTRODUCTION

In recent years the importance of multiple scattering in low-energy electron diffraction (LEED) has been well documented, both experimentally and theoretically. However, many cases do exist in which the experimental results can be analyzed largely within the framework of a single scattering, or kinematic theory. In the course of recent LEED studies<sup>1</sup> of the (110) surface of chromium, the energy dependence of the diffracted intensity was found to be in striking agreement with kinematic predictions. Since a large number of diffraction beams was studied, an orderly procedure for analyzing the intensity spectra was sought. The procedure developed is described herein. It provides a ready means for predicting the energies at which kinematic intensity maxima, the so-called "Bragg" peaks, will be observed. Additionally, it provides a method for plotting all of the intensity data for a given crystal on a single universal curve, determining in the process the inner potential correction and the lattice parameter near the surface. The calculation described in this report is restricted to the case of normal electron beam incidence. However, this condition can be relaxed, at the cost of additional complexity, and the extension of the calculation to non-normal incidence proceeds in a straightforward, if algebraically complicated, manner.

The procedure and equations used in the analysis are presented in Section II. Since excellent published reviews<sup>2,3</sup> of many aspects of LEED are available, a minimum of background material is included. Results for various low-index surfaces of the bcc and fcc structures are given in Sections III and IV respectively. The application to the analysis of experimental results is demonstrated in Section V, for the (110) surface

of the bcc crystal chromium, and the (100) surface of the fcc crystal aluminum. Section VI concludes with a brief discussion of the general applicability of the method as presented.

## II. DIFFRACTION EQUATIONS AND PROCEDURE

The treatment is confined to the elastic back-scattering of electrons incident on a crystal normal to its surface. The incident and diffracted electrons are characterized by wave vectors  $\vec{k}_0$  and  $\vec{k}$ , respectively, while  $\vec{G}$  is a reciprocal lattice vector determined by the full three-dimensional periodicity of the crystal. The relationship of these vectors and  $\theta$ , the angle of diffraction, is indicated in Fig. 1. Conservation of momentum and energy in the diffraction process impose, respectively, the following conditions:

$$\vec{k} = \vec{k}_0 + \vec{G}, \quad (1)$$

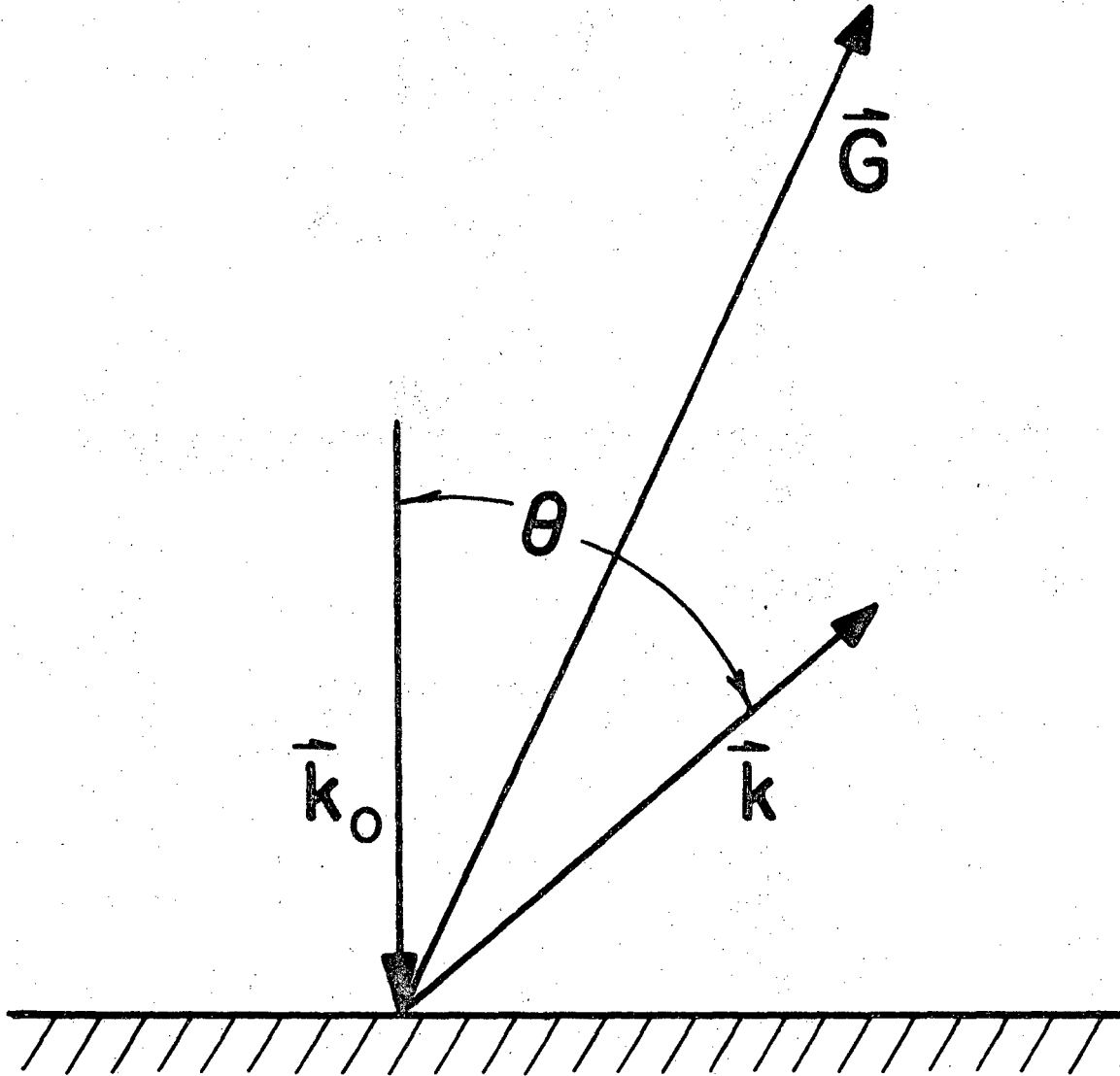
$$|k| = |k_0| = \frac{1}{\lambda'} = \left\{ \frac{V'}{150.4} \right\}^{1/2}, \quad (2)$$

where the magnitudes of the electron wavevectors have been expressed in terms of the de Broglie wavelength  $\lambda'$  and energy  $V'$  of the electrons outside the crystal. The units of length and energy are A and eV, respectively. Squaring Eq. (1) and noting that  $\vec{k}_0$  is normal to the surface,

$$2\vec{k}_0 \cdot \vec{G} + |G|^2 = 2|k_0| |G_1| + |G|^2 = 0, \quad (3)$$

where  $\vec{G}_1$  is the normal component of  $\vec{G}$ . The component parallel to the surface will be written  $\vec{G}_\parallel$ . The polar angle  $\phi$  and diffraction angle  $\theta$  which define the directions of the beams of diffracted electrons are determined by the parallel projection of Eq. (1):

$$\vec{k}_\parallel = \vec{G}_\parallel. \quad (4)$$



XBL707-3461

Fig. 1. Showing the relationship between the wave vectors  $\vec{k}_0$  and  $\vec{k}$ , the reciprocal lattice vector  $\vec{G}$ , and the diffraction angle  $\theta$ , for normal incidence.

Values of  $\phi$  are discrete, since  $\vec{G}_{\parallel}$  can assume only those directions in the surface which are permitted by the surface periodicity. However, for any given value of  $\vec{G}_{\parallel}$ ,  $\theta$  varies continuously with  $\lambda'$  or  $V'$ . From Eqs. (2) and (4), and writing  $|k_{\parallel}| = |k_0| \sin\theta$ ,

$$(V')^{1/2} \sin\theta = \sqrt{150.4} |G_{\parallel}|. \quad (5)$$

In comparing the observed and calculated relationships between  $V'$  and  $\theta$ , it may be assumed that the incident electrons remain outside the crystal. On the other hand, the energy dependence of the diffracted intensity arises mainly from the penetration of the incident electrons into the crystal. Inside, the electrons' energy  $V$  differs from that outside by the so-called inner potential,  $V_0$ :

$$V = V' - V_0,$$

where  $V_0$  is generally an attractive potential, of order -10 to -20 eV for metals. Thus it may be expected that corresponding features in the calculated and observed intensities will occur at energies which differ by  $V_0$ . For  $V'$  greater than about 50 eV,  $V_0$  is nearly independent of energy.<sup>3</sup>

It will be assumed that the energy values at which intensity maxima occur for a particular diffraction beam, may be calculated solely from the phase relationships between electrons scattered by all of the atoms in the crystal. Only single scattering will be considered, and attenuation of the incident electron beam inside the crystal will be ignored. Combining Eq. (3), the condition for diffraction including the full three-dimensional periodicity of the crystal, with Eq. (2) for electrons of

energy  $V = V' - V_0$  inside the crystal, yields

$$V_{\max} = (V'_{\max} - V_0) = \frac{150.4}{4} \left\{ \frac{|G|^2}{|G_1|} \right\}^2 \quad (6)$$

The energies  $V_{\max}$  at which intensity maxima are predicted are readily calculated, once  $|G|$  and  $|G_1|$  are known for the crystal structure and surface of interest. It is convenient to rewrite Eq. (6) in terms of a new function,  $F$ , and the experimentally controlled energy,  $V'$ , as follows:

$$V'_{\max} = V_0 + \left( \frac{37.6}{a_0^2} \right) F, \quad (7a)$$

$$F \equiv a_0^2 \left\{ \frac{|G|^2}{|G_1|} \right\}^2, \quad (7b)$$

where  $a_0$  is the lattice parameter associated with the x-ray unit cell. Equations (7) are written in a form that is valid for cubic crystals. A comparable formulation is possible for non-cubic crystals, and for those requiring more than one lattice parameter. The function  $F$  as defined in Eq. (7b) is independent of  $a_0$ , since the quantity in curly brackets contains the factor  $1/a_0^2$ . In this form,  $F$  is the same for all crystals having the given structure and surface.

Analysis of intensity data entails plotting experimentally determined values of  $V'_{\max}$  vs calculated values of  $F$  for all diffraction beams from a given surface, and for different surfaces of the same crystal if  $V_0$  is isotropic. If the indexing of the intensity maxima is correct and the single scattering model is appropriate, all of the data points will lie on a single straight line, according to Eq. (7a). The slope of this line, and its intercept at  $F=0$ , determine  $a_0$  and  $V_0$  respectively. This

procedure will be followed in the analysis of intensity data in Section V.

Since the quantities  $\vec{G}_{\parallel}$  and  $\vec{G}_{\perp}$  are required in Eqs. (4) and (7b), it is most convenient to be able to express  $\vec{G}$  in terms of reciprocal lattice basis vectors, two of which lie in the surface of interest, and one normal to the surface. It is always possible to define two basis vectors  $\vec{R}_1, \vec{R}_2$  parallel to the surface in such a manner that

$$\vec{G}_{\parallel} = \{n_1 \vec{R}_1 + n_2 \vec{R}_2\} .$$

The indices  $n_1, n_2$ , which are positive or negative integers or zero, identify the various LEED beams in the usual manner. Equation (4) then determines the angles which define the positions of the  $(n_1 n_2)$  beams. If for the crystal structure and surface of interest, atoms in all planes parallel to the surface lie directly beneath the surface atoms, then  $\vec{R}_3$  may be defined so that  $\vec{G}_{\perp} = n_3 \vec{R}_3$ . More generally this condition is not met, with the result that  $\vec{G}_{\perp}$  must be written

$$\vec{G}_{\perp} = f(n_1, n_2, n_3) \vec{R}_3 .$$

The function  $f(n_1, n_2, n_3)$  is determined by the choice of crystal structure and surface.

Various procedures may be followed in defining  $\vec{R}_1, \vec{R}_2$ , and  $\vec{R}_3$ , and obtaining the function  $f(n_1, n_2, n_3)$ . In the present work, the reciprocal lattice is first defined in terms of the usual x-ray unit cell of the crystal structure under consideration. Then for each surface of interest, a transformation is effected which leaves  $\vec{G}$  in the required form,

$$\begin{aligned}\vec{G}(n_1, n_2, n_3) &= \vec{G}_{\parallel} + \vec{G}_{\perp} \\ &= \{n_1 \vec{R}_1 + n_2 \vec{R}_2\} + f(n_1, n_2, n_3) \vec{R}_3.\end{aligned}$$

Equations (4), (5), and (7) may then be used to characterize the diffraction of low energy electrons, within the kinematic or single scattering framework.

The advantages of the method for the kinematical analysis of LEED data described in this report are the following. All LEED beams from a given surface and crystal structure may be characterized once the appropriate expressions for  $\vec{G}(n_1, n_2, n_3)$  and  $F(n_1, n_2, n_3)$  have been obtained. Indexing of the intensity maxima is convenient and descriptive of the various beams. Intensity data for all of the beams from a given material lie on a single universal straight line which determines the inner potential and lattice parameter values. The expressions derived for  $\vec{G}(n_1, n_2, n_3)$  and  $F(n_1, n_2, n_3)$  are immediately applicable to the appropriate surface of any crystal having the given structure. Extension of the method to non-normal electron beam incidence, or non-cubic crystal structures, is straightforward.

### III. RESULTS FOR bcc CRYSTAL STRUCTURE

A choice of primitive translation vectors for the bcc structure, illustrated in Fig. 2, is

$$\vec{a} = \frac{a_0}{2} (\hat{x} + \hat{y} - \hat{z}), \quad \vec{b} = \frac{a_0}{2} (-\hat{x} + \hat{y} + \hat{z}), \quad \vec{c} = \frac{a_0}{2} (\hat{x} - \hat{y} + \hat{z})$$

where  $\hat{x}$ ,  $\hat{y}$ ,  $\hat{z}$  are unit vectors. The corresponding translation vectors of the reciprocal lattice are

$$\vec{A} = \frac{1}{a_0} (\hat{x} + \hat{y}), \quad \vec{B} = \frac{1}{a_0} (\hat{y} + \hat{z}), \quad \vec{C} = \frac{1}{a_0} (\hat{x} + \hat{z}).$$

The vector which spans all points of the reciprocal lattice is

$$\begin{aligned} \vec{G}(h,k, \ell) &= h\vec{A} + k\vec{B} + \ell\vec{C} \\ &+ \frac{1}{a_0} \left\{ (h + \ell) \hat{x} + (h + k)\hat{y} + (k + \ell) \hat{z} \right\}. \end{aligned}$$

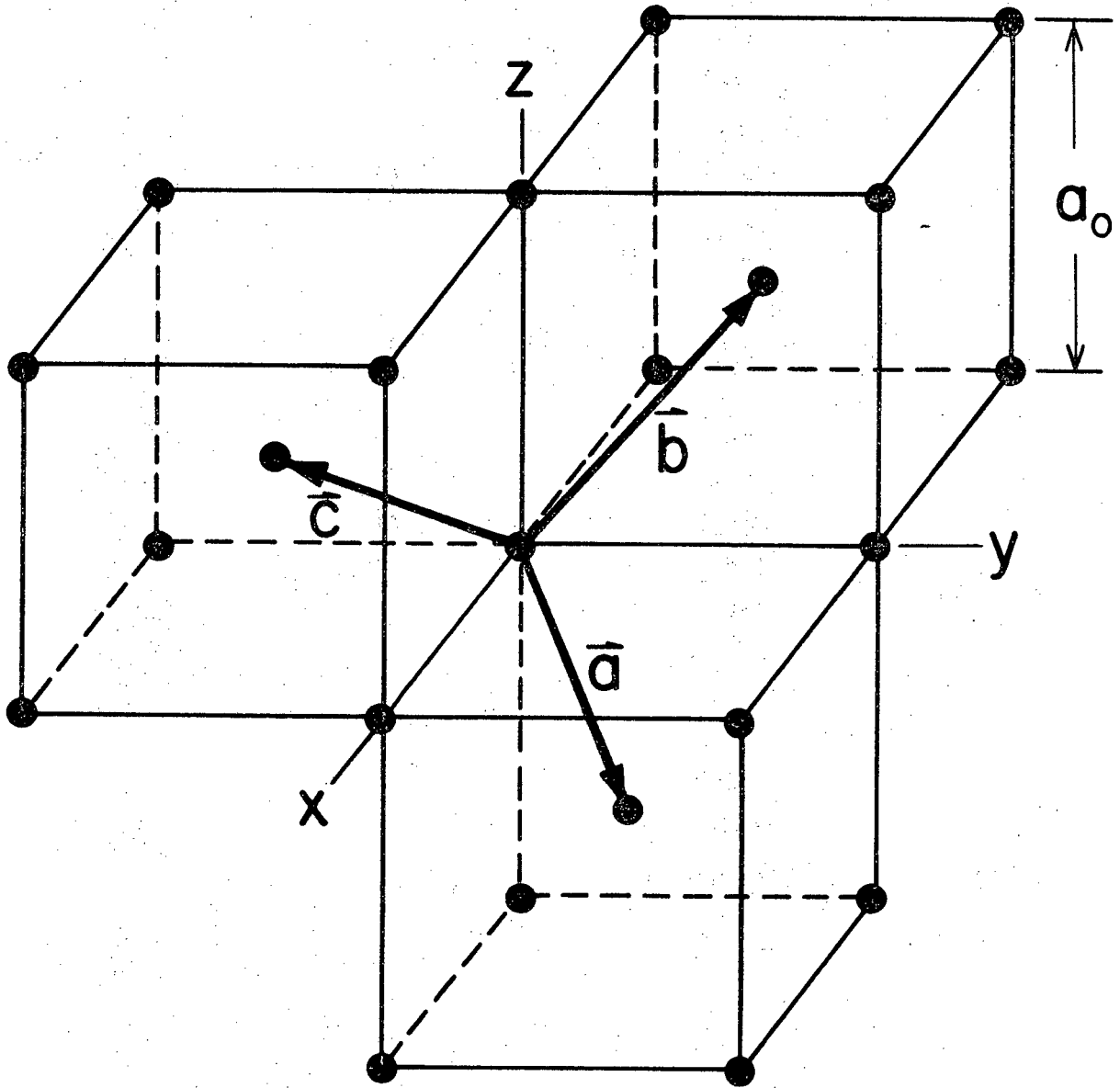
The bcc surfaces to be considered are shown in Fig. 3. The first of the following calculations for particular surfaces will be described in some detail, in order to indicate the method used. A much briefer description will be given for the remaining surfaces.

#### A. (110) Surface

The unit vector normal to the (110) surface illustrated in Fig. 3 is

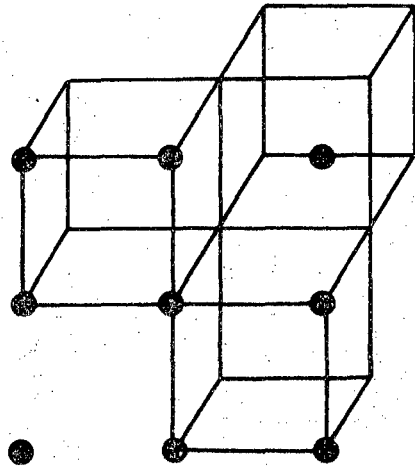
$$\hat{N} = \frac{\hat{x} + \hat{y}}{\sqrt{2}}$$

The basis vectors  $\vec{A}$ ,  $\vec{B}$ ,  $\vec{C}$ , may be written in terms of components parallel and perpendicular to  $\hat{N}$ , with the result

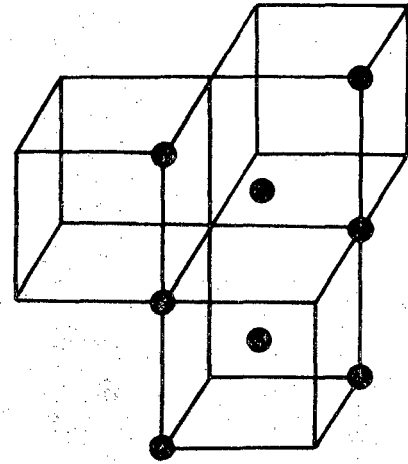


XBL707-3467

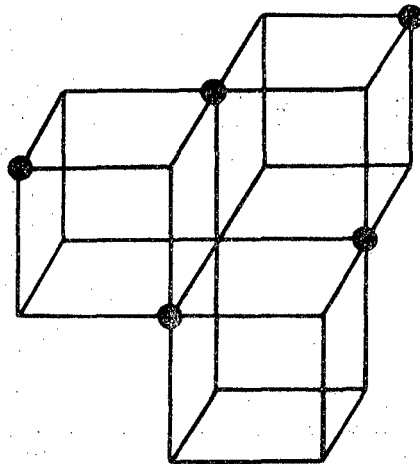
Fig. 2. The bcc lattice structure, showing three primitive translation vectors.



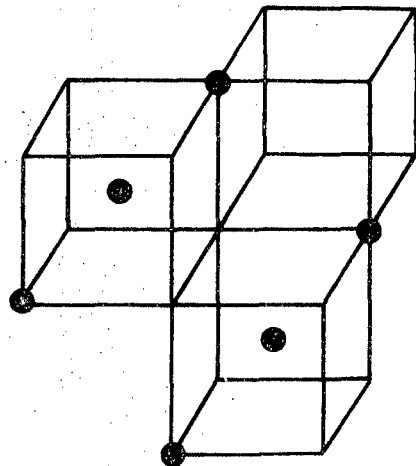
(100)



(110)



(111)



(211)

XBL707-3464

Fig. 3. The four surfaces of the bcc structure for which calculations have been made. Atoms lying in these surfaces are shown.

$$\begin{aligned} \vec{A}_{\parallel} &= 0, & \vec{A}_{\perp} &= \frac{1}{a_0} (\hat{x} + \hat{y}) ; \\ \vec{B}_{\parallel} &= \frac{1}{2a_0} (-\hat{x} + \hat{y} + 2\hat{z}), & \vec{B}_{\perp} &= \frac{1}{2a_0} (\hat{x} + \hat{y}) ; \\ \vec{C}_{\parallel} &= \frac{1}{2a_0} (\hat{x} - \hat{y} + 2\hat{z}), & \vec{C}_{\perp} &= \frac{1}{2a_0} (\hat{x} + \hat{y}) ; \end{aligned}$$

$$\begin{aligned} \vec{G}(h,k,\ell) &= h(\vec{A}_{\parallel} + \vec{A}_{\perp}) + k(\vec{B}_{\parallel} + \vec{B}_{\perp}) + \ell(\vec{C}_{\parallel} + \vec{C}_{\perp}) \\ &= \frac{1}{2a_0} \left\{ k(-\hat{x} + \hat{y} + 2\hat{z}) + \ell(\hat{x} - \hat{y} + 2\hat{z}) + [2h+k+\ell](\hat{x} + \hat{y}) \right\} . \end{aligned}$$

The choice for directions of the new basis vectors  $\vec{R}_1, \vec{R}_2, \vec{R}_3$  is evident from the last equation above. It is useful to express  $\vec{R}_1, \vec{R}_2, \vec{R}_3$  as products of two factors, as follows:

$$\vec{R}_1 = \frac{\sqrt{3}}{\sqrt{2} a_0} \left[ \frac{-\hat{x} + \hat{y} + 2\hat{z}}{\sqrt{6}} \right], \quad \vec{R}_2 = \frac{\sqrt{3}}{\sqrt{2} a_0} \left[ \frac{-\hat{x} + \hat{y} - 2\hat{z}}{\sqrt{6}} \right], \quad \vec{R}_3 = \frac{\sqrt{2}}{a_0} \left[ \frac{\hat{x} + \hat{y}}{2} \right].$$

The quantities in square brackets are unit vectors, with the directions of  $\vec{R}_1$  and  $\vec{R}_2$  chosen so as to define an angle greater than  $90^\circ$ , in accordance with the normal convention.<sup>4</sup> The magnitudes of  $\vec{R}_1$  and  $\vec{R}_2$  are the reciprocal separations of lines of atoms in the surface normal to the directions of  $\vec{R}_1$  and  $\vec{R}_2$  respectively. The magnitude of  $\vec{R}_3$  is the reciprocal separation of planes of atoms parallel to the surface. In terms of  $\vec{R}_1, \vec{R}_2, \vec{R}_3$ ,  $\vec{G}(h,k, \ell)$  may be written

$$\vec{G}(h,k, \ell) = k\vec{R}_1 - \ell\vec{R}_2 + \frac{1}{2} (2h+k+\ell) \vec{R}_3 .$$

Defining  $n_1, n_2, n_3$  yields finally

$$n_1 = k, n_2 = -l, n_3 = h ;$$

$$\vec{G}(n_1, n_2, n_3) = \{n_1 \vec{R}_1 + n_2 \vec{R}_2\} + \frac{1}{2}(n_1 - n_2 + 2n_3) \vec{R}_3 .$$

Substitution in Eqs. (5) and (7b) gives

$$(v')^{1/2} \cdot \sin\theta = \frac{\sqrt{150.4}}{\sqrt{2} a_0} \left\{ (n_1 + n_2)^2 + 2(n_1 - n_2)^2 \right\}^{1/2} ;$$

$$F = \left\{ \frac{(n_1 + n_2)^2 + 2(n_1 - n_2)^2 + (n_1 - n_2 + 2n_3)^2}{n_1 - n_2 + 2n_3} \right\}^2 .$$

The basis vectors  $\vec{R}_1, \vec{R}_2$  are shown in Fig. 4, together with the indexing of the diffraction beams and their orientation relative to the crystal axes.

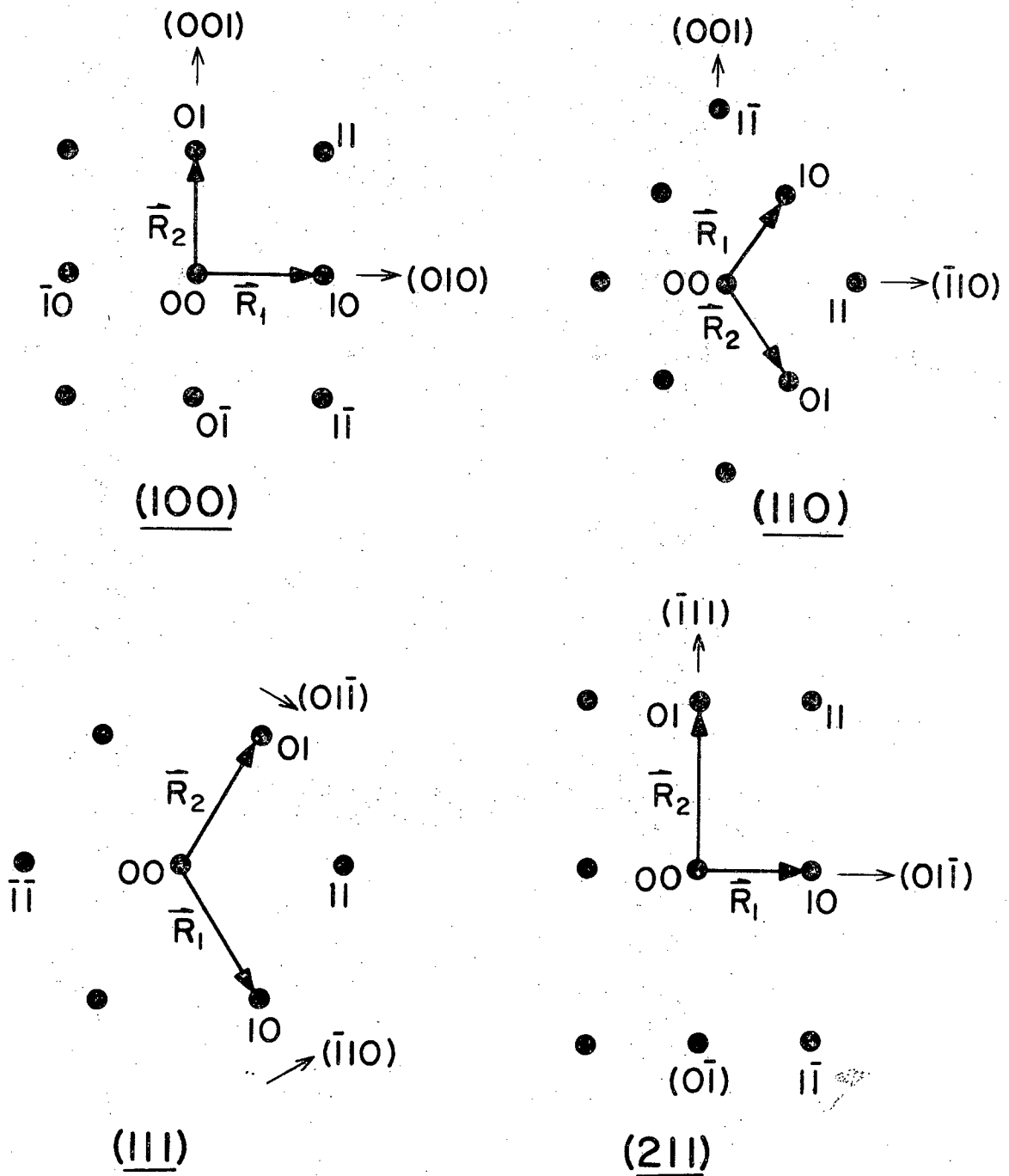
#### B. (100) Surface

For the (100) surface illustrated in Fig. 3, the unit vector normal to the surface is  $\hat{N} = \hat{x}$ . The separation of planes of atoms parallel to the surface is  $a_0/2$ . Since  $\vec{G}(h,k,l)$  is already in the form  $\vec{G} = \vec{G}_{\parallel} + \vec{G}_{\perp}$ , the required transformation is apparent:

$$\vec{R}_1 = \frac{1}{a_0} [\hat{y}], \quad \vec{R}_2 = \frac{1}{a_0} [\hat{z}], \quad \vec{R}_3 = \frac{2}{a_0} [\hat{x}] ;$$

$$n_1 = h+k, \quad n_2 = k+l, \quad n_3 = l ;$$

$$\vec{G}(n_1, n_2, n_3) = \{n_1 \vec{R}_1 + n_2 \vec{R}_2\} + \frac{1}{2}(n_1 - n_2 + 2n_3) \vec{R}_3$$



XBL707-3458

Fig. 4. The surface reciprocal lattice basis vectors and LEED indexing for the four bcc surfaces shown in Fig. 3.

The assignment  $n_3 = \ell$  is arbitrary to the extent that the choice  $n_3 = h$  or  $n_3 = k$  would yield comparable results, the difference being in the values of  $n_3$  which yield the same intensity peak for, say, the (10), ( $\bar{1}0$ ), (01), and (0 $\bar{1}$ ) beams. The restriction on  $n_3$  is that it be set equal to just one of the integers  $h, k, \ell$ . Substitution for  $\vec{G}$ ,  $\vec{G}_{\parallel}$ , and  $\vec{G}_{\perp}$  in Eqs. (5) and (7b) yields

$$(V')^{1/2} \sin\theta = \frac{\sqrt{150.4}}{a_0} \{n_1^2 + n_2^2\}^{1/2},$$

$$F = \left\{ \frac{n_1^2 + n_2^2 + (n_1 - n_2 + 2n_3)^2}{n_1 - n_2 + 2n_3} \right\}^2.$$

The basis vectors and beam indexing are illustrated in Fig. 4.

### C. (111) Surface

The unit normal vector is  $\hat{N} = (\hat{x} + \hat{y} + \hat{z})/\sqrt{3}$ , and the separation of planes of atoms parallel to the surface is  $a_0/(2\sqrt{3})$ . The required transformation is

$$\vec{R}_1 = \frac{\sqrt{2}}{\sqrt{3} a_0} \begin{bmatrix} \hat{x} + \hat{y} - 2\hat{z} \\ \sqrt{6} \end{bmatrix}, \quad \vec{R}_2 = \frac{2}{\sqrt{3} a_0} \begin{bmatrix} \hat{y} + \hat{z} - 2\hat{x} \\ \sqrt{6} \end{bmatrix}, \quad \vec{R}_3 = \frac{2\sqrt{3}}{a_0} \begin{bmatrix} \hat{x} + \hat{y} + \hat{z} \\ \sqrt{3} \end{bmatrix}$$

$$n_1 = h - \ell, \quad n_2 = k - \ell, \quad n_3 = \ell;$$

$$\vec{G}(n_1, n_2, n_3) = \{n_1 \vec{R}_1 + n_2 \vec{R}_2\} + \frac{1}{3} (n_1 + n_2 + 3n_3) \vec{R}_3$$

and applying Eqs. (5) and (7b),

$$(V')^{1/2} \sin \theta = \frac{\sqrt{150.4}}{\sqrt{3} a_0} \left\{ n_1^2 + n_2^2 + (n_1 - n_2)^2 \right\}^{1/2} ;$$

$$F = \frac{1}{12} \left\{ \frac{n_1^2 + n_2^2 + (n_1 - n_2)^2 + 4(n_1 + n_2 + 3n_3)^2}{n_1 + n_2 + 3n_3} \right\}^2$$

The basis vectors and indexing are shown in Fig. 4.

#### D. (211) Surface

The unit normal vector  $\hat{N} = (2\hat{x} + \hat{y} + \hat{z})/\sqrt{6}$ , and the separation of atomic planes parallel to the surface is  $a_0/\sqrt{6}$ . The required transformation is

$$\vec{R}_1 = \frac{1}{\sqrt{2} a_0} \begin{bmatrix} \hat{y} - \hat{z} \\ \sqrt{2} \end{bmatrix}, \quad \vec{R}_2 = \frac{2}{\sqrt{3} a_0} \begin{bmatrix} -\hat{x} + \hat{y} + \hat{z} \\ \sqrt{3} \end{bmatrix}, \quad \vec{R}_3 = \frac{\sqrt{6}}{a_0} \begin{bmatrix} 2\hat{x} + \hat{y} + \hat{z} \\ \sqrt{6} \end{bmatrix}$$

$$n_1 = h - \ell, \quad n_2 = k, \quad n_3 = \ell ;$$

$$\vec{G}(n_1, n_2, n_3) = \{n_1 \vec{R}_1 + n_2 \vec{R}_2\} + \frac{1}{6} (3n_1 + 2n_2 + 6n_3) \vec{R}_3 .$$

Finally,

$$(V')^{1/2} \sin \theta = \frac{\sqrt{150.4}}{\sqrt{6} a_0} \left\{ 3n_1^2 + 8n_2^2 \right\}^{1/2} ;$$

$$F = \frac{1}{6} \left\{ \frac{3n_1^2 + 8n_2^2 + (3n_1 + 2n_2 + 6n_3)^2}{3n_1 + 2n_2 + 6n_3} \right\}^2 .$$

## IV. RESULTS FOR fcc CRYSTAL STRUCTURE

A choice of primitive translation vectors for the fcc structure (see Fig. 5) is

$$\vec{a} = \frac{a_0}{2} (\hat{x} + \hat{y}), \quad \vec{b} = \frac{a_0}{2} (\hat{y} + \hat{z}), \quad \vec{c} = \frac{a_0}{2} (\hat{x} + \hat{z}).$$

The corresponding translation vectors of the reciprocal lattice are

$$\vec{A} = \frac{1}{a_0} (\hat{x} + \hat{y} - \hat{z}), \quad \vec{B} = \frac{1}{a_0} (-\hat{x} + \hat{y} + \hat{z}), \quad \vec{C} = \frac{1}{a_0} (\hat{x} - \hat{y} + \hat{z})$$

and the general reciprocal lattice vector is

$$\begin{aligned} G(h,k,\ell) &= h\vec{A} + k\vec{B} + \ell\vec{C} \\ &= \frac{1}{a_0} \left\{ (h-k+\ell)\hat{x} + (h+k-\ell)\hat{y} + (-h+k+\ell)\hat{z} \right\}. \end{aligned}$$

The fcc surfaces to be considered are shown in Fig. 6.

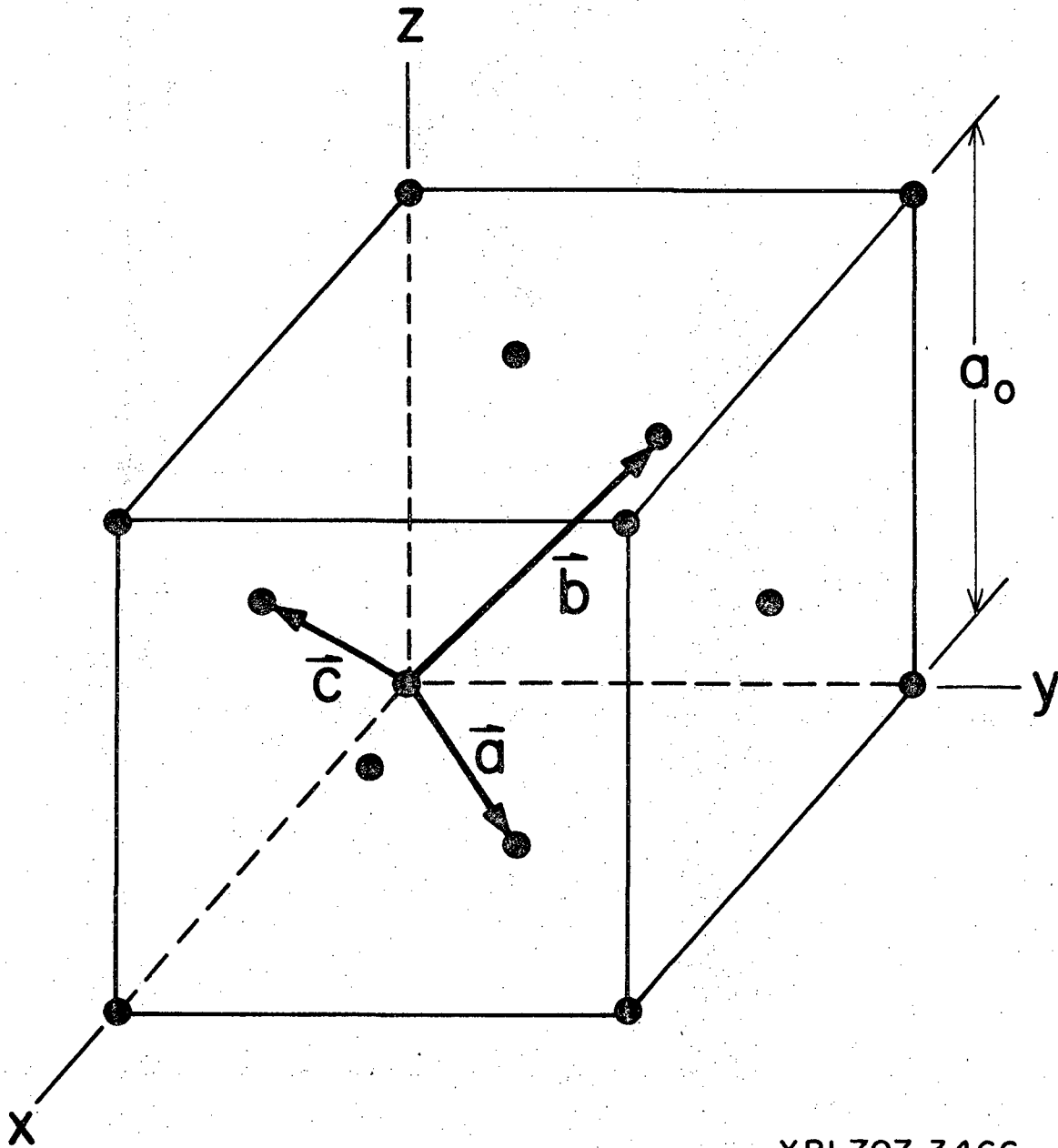
A. (100) Surface

The unit normal vector is  $\hat{N} = \hat{x}$ , and the separation of planes of atoms parallel to the surface is  $a_0/2$ . The required transformation is

$$\vec{R}_1 = \frac{\sqrt{2}}{a_0} \begin{bmatrix} \hat{y}-\hat{z} \\ \sqrt{2} \end{bmatrix}, \quad \vec{R}_2 = \frac{\sqrt{2}}{a_0} \begin{bmatrix} \hat{y}+\hat{z} \\ \sqrt{2} \end{bmatrix}, \quad \vec{R}_3 = \frac{\sqrt{2}}{a_0} [\hat{x}] ;$$

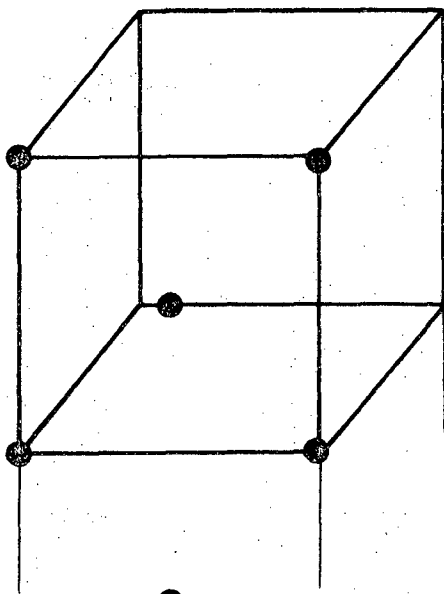
$$n_1 = h-\ell, \quad n_2 = k, \quad n_3 = \ell ;$$

$$\vec{G}(n_1, n_2, n_3) = \{ n_1\vec{R}_1 + n_2\vec{R}_2 \} + \frac{1}{2} (n_1 - n_2 + 2n_3)\vec{R}_3 .$$

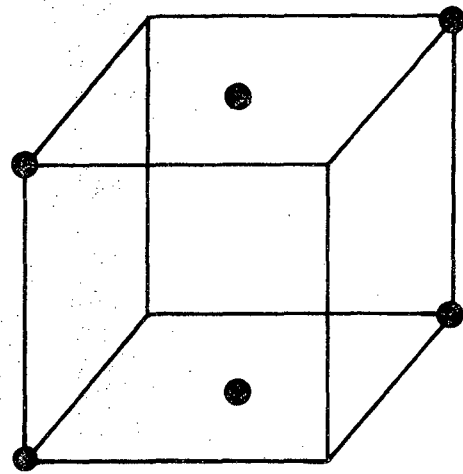


XBL707-3466

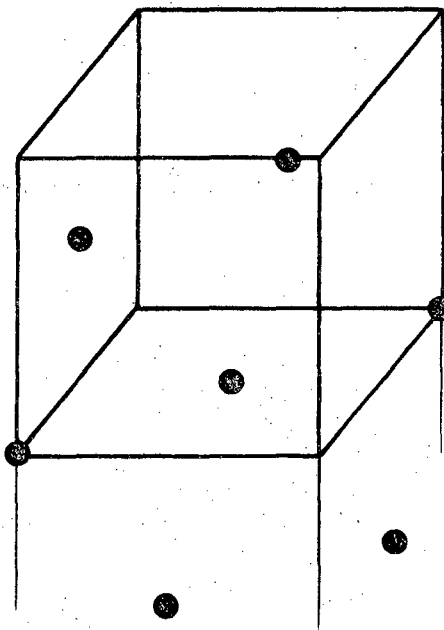
Fig. 5. The fcc lattice structure, showing three primitive translation vectors.



(100)



(110)



(111)

XBL707-3465

Fig. 6. The three surfaces of the fcc structure for which calculations have been made. Atoms lying in these surfaces are shown.

Thus

$$(V')^{1/2} \sin\theta = \sqrt{150.4} \frac{\sqrt{2}}{a_0} \{n_1^2 + n_2^2\}^{1/2} ;$$

$$F = \left\{ \frac{2n_1^2 + 2n_2^2 + (n_1 - n_2 + 2n_3)^2}{n_1 - n_2 + 2n_3} \right\}^2$$

The basis vectors  $\vec{R}_1, \vec{R}_2$ , and the diffraction beam indexing for the fcc surfaces treated, are shown in Fig. 7.

#### B. (110) Surface

The unit normal vector has the value  $\hat{N} = (\hat{x} + \hat{y})/\sqrt{2}$ , and the spacing of atomic planes parallel to the surface is  $a_0/(2\sqrt{2})$ . The results are as follows:

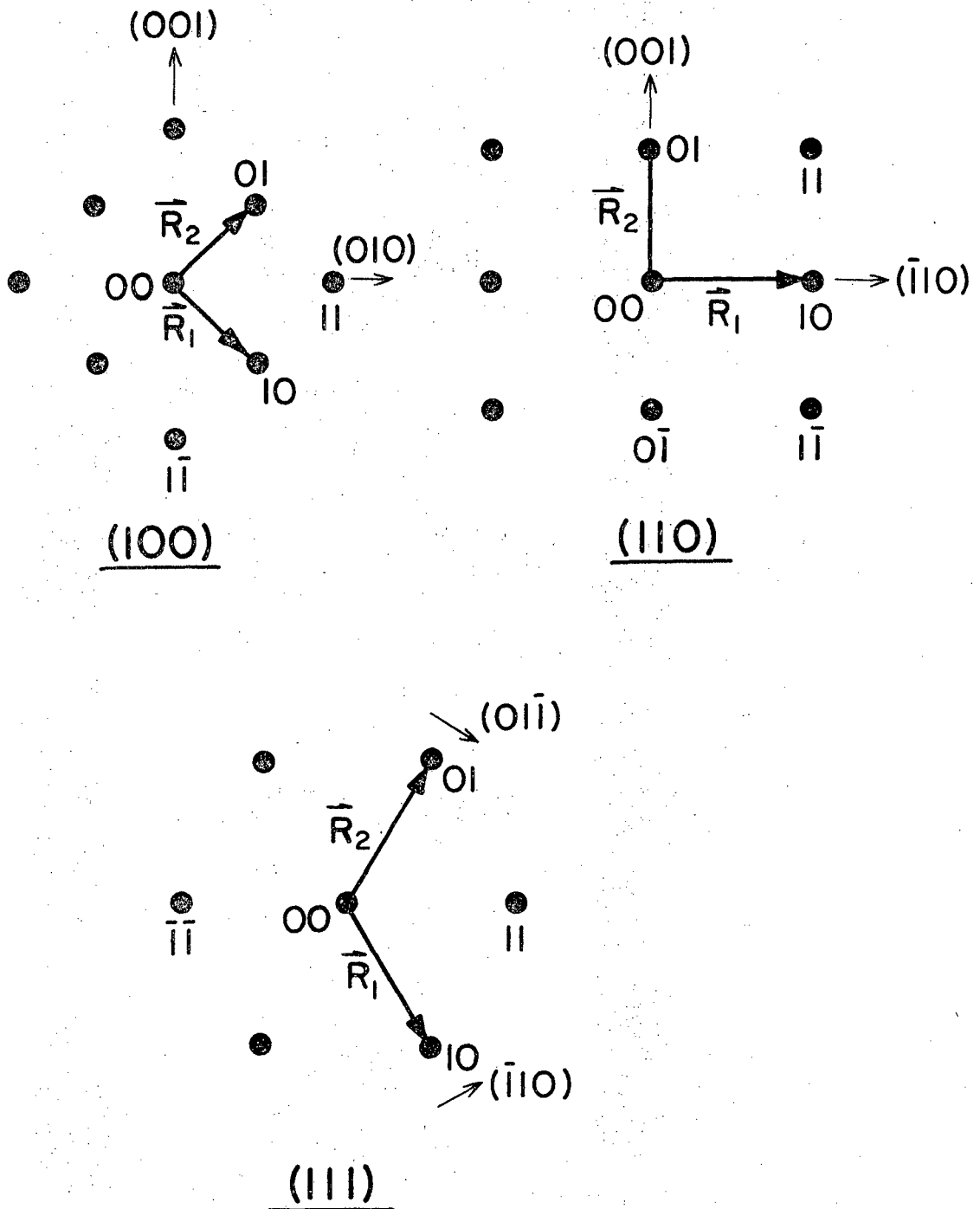
$$\vec{R}_1 = \frac{\sqrt{2}}{a_0} \left[ \frac{\hat{y} - \hat{x}}{\sqrt{2}} \right], \quad \vec{R}_2 = \frac{1}{a_0} [\hat{z}], \quad \vec{R}_3 = \frac{2\sqrt{2}}{a_0} \left[ \frac{\hat{x} + \hat{y}}{\sqrt{2}} \right];$$

$$n_1 = k - l, \quad n_2 = -h + k + l, \quad n_3 = l;$$

$$\vec{G}(n_1, n_2, n_3) = \{ n_1 \vec{R}_1 + n_2 \vec{R}_2 \} + \frac{1}{2} (n_1 - n_2 + 2n_3) \vec{R}_3 ;$$

$$(V')^{1/2} \sin\theta = \frac{\sqrt{150.4}}{a_0} \{2n_1^2 + n_2^2\}^{1/2} ;$$

$$F = \frac{1}{2} \left\{ \frac{2n_1^2 + n_2^2 + 2(n_1 - n_2 + 2n_3)^2}{n_1 - n_2 + 2n_3} \right\}^2$$



XBL707-3463

Fig. 7. Surface reciprocal lattice basis vectors and LEED indexing for the three fcc surfaces shown in Fig. 6.

C. (111) Surface

The unit normal vector is  $N = (x + y + z)/\sqrt{3}$ , while the spacing of planes of atoms parallel to the surface is  $a_0/\sqrt{3}$ . The results are as follows:

$$\vec{R}_1 = \frac{2\sqrt{2}}{\sqrt{3} a_0} \left[ \frac{\hat{x} + \hat{y} - 2\hat{z}}{\sqrt{6}} \right], \quad \vec{R}_2 = \frac{2\sqrt{2}}{\sqrt{3} a_0} \left[ \frac{-2\hat{x} + \hat{y} + \hat{z}}{\sqrt{6}} \right], \quad \vec{R}_3 = \frac{\sqrt{3}}{a_0} \left[ \frac{\hat{x} + \hat{y} + \hat{z}}{\sqrt{3}} \right];$$

$$n_1 = h - \ell, \quad n_2 = k - \ell, \quad n_3 = \ell;$$

$$\vec{G}(n_1, n_2, n_3) = \{n_1 \vec{R}_1 + n_2 \vec{R}_2\} + \frac{1}{3} (n_1 + n_2 + 3n_3) \vec{R}_3;$$

$$(v')^{1/2} \sin\theta = \sqrt{150.4} \frac{2}{\sqrt{3} a_0} \left\{ n_1^2 + n_2^2 + (n_1 - n_2)^2 \right\}^{1/2};$$

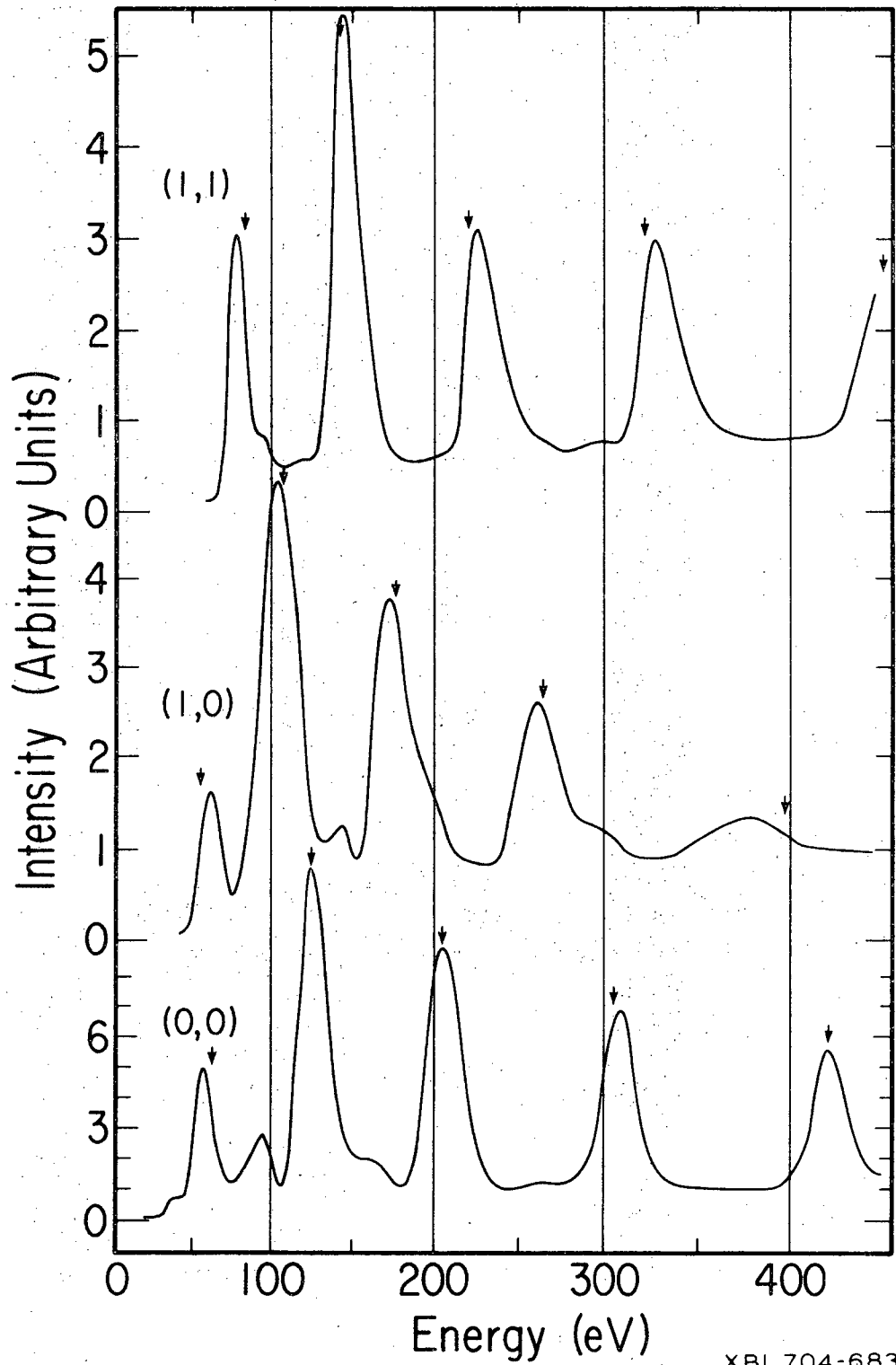
$$F = \frac{16}{3 a_0^2} \left\{ \frac{n_1^2 + n_2^2 + (n_1 - n_2)^2 + \frac{1}{4} (n_1 + n_2 + 3n_3)^2}{n_1 + n_2 + 3n_3} \right\}^2$$

## V. ANALYSIS OF INTENSITY SPECTRA: Cr(110) AND Al(100)

If a single-scattering analysis of LEED intensity is appropriate to a given material, the intensity spectrum for each diffraction beam contains a small number of prominent peaks, and subsidiary structure is considerably weaker. The correct indexing of the intensity peaks may be obtained by comparing the observed values of  $V'_{\max}$  with values of  $V_{\max}$  calculated from Eqs. (6), (7b), and the appropriate expressions for  $F(n_1, n_2, n_3)$  using the bulk lattice parameter  $a_0$ . A shift of all values of  $V'_{\max}$  should bring the latter into reasonable coincidence with the calculated  $V_{\max}$  values; the shift represents the inner potential correction. Every intensity peak is thus characterized by a set of values for  $n_1$ ,  $n_2$ , and  $n_3$ ;  $n_1$  and  $n_2$  identify the diffraction beam, while  $n_3$  is the integer that yields agreement between  $(V'_{\max} - V_0)$  and  $V_{\max}$ . Once the intensity peaks have been indexed, the observed  $V'_{\max}(n_1, n_2, n_3)$  may be plotted vs  $F(n_1, n_2, n_3)$ . The points should lie on a single straight line according to Eq. (7a). The intercept at  $F=0$  yields  $V_0$ , and the slope determines  $a_0$ . As examples of the foregoing procedure, the analysis of intensity data for the bcc crystal chromium and the fcc crystal aluminum will be described.

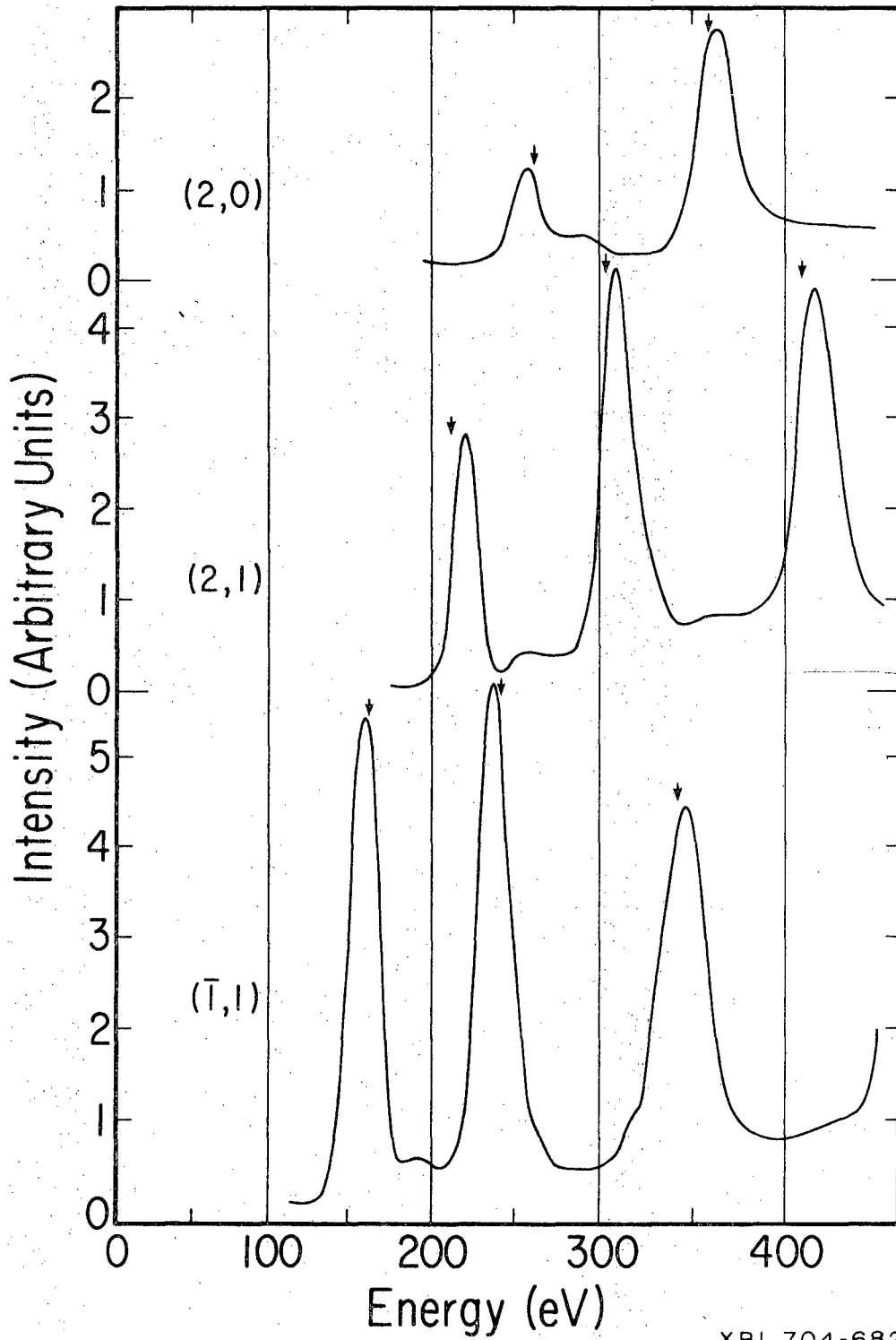
### A. Cr(110)

Intensity spectra for six diffraction beams from the (110) surface of chromium are shown in Figs. 8 and 9. The data<sup>1</sup> were obtained with a conventional post-acceleration LEED apparatus and telephotometer. Values of  $V'_{\max}$  were determined by averaging over several runs for each diffraction beam.



XBL 704-683

Fig. 8. Intensity spectra for the (00), (10), and (11) diffraction beams from the (110) surface of chromium. The angle of incidence was  $86^\circ$  for the specular beam, and  $90^\circ$  for the others. Arrows indicate the values of  $(V_{max} + V_0)$  obtained in the analysis.



XBL 704-682

Fig. 9. Intensity spectra for the (11), (21), and (20) diffraction beams from the (110) surface of chromium. The angle of incidence was  $90^\circ$ . Arrows indicate the values of  $(V_{\max} + V_0)$  obtained in the analysis.

For the (110) surface of a bcc crystal, the results obtained in Section III predict intensity maxima for

$$V_{\max} = (V'_{\max} - V_0) = \frac{37.6}{a_0} F(n_1, n_2, n_3); \quad (8)$$

$$F(n_1, n_2, n_3) = \frac{1}{2} \left\{ \frac{(n_1+n_2)^2 + 2(n_1-n_2)^2 + (n_1-n_2+2n_3)^2}{n_1-n_2+2n_3} \right\}^2. \quad (9)$$

Expanding Eq. (9) for the diffraction beams  $(n_1, n_2)$  studied experimentally yields the following results:

$$(00): \quad F = 2n_3^2$$

$$(10): \quad F = \frac{1}{2} \left\{ \frac{3+(1+2n_3)^2}{1+2n_3} \right\}^2,$$

$$(11): \quad F = 2 \left\{ \frac{1+n_3^2}{n_3} \right\}^2,$$

$$(\bar{1}1): \quad F = 2 \left\{ \frac{2+(n_3-1)^2}{n_3-1} \right\}^2,$$

$$(12): \quad F = \frac{1}{2} \left\{ \frac{11+(2n_3-1)^2}{2n_3-1} \right\}^2,$$

$$(02): \quad F = 2 \left\{ \frac{3+(n_3-1)^2}{n_3-1} \right\}^2,$$

$$(22): \quad F = 2 \left\{ \frac{4+n_3^2}{n_3} \right\}^2.$$

These expressions were used to calculate  $F(n_1, n_2, n_3)$  as listed in Table I. The indexing of the experimental  $V'_{\max}$  values was then determined by

Table I. Values of  $F$ ,  $V'_{\max}$  and  $(V_{\max} + V_0)$  obtained for the intensity maxima in LEED studies of the (110) surface of chromium. Only integral order maxima are considered. Energies are in eV.

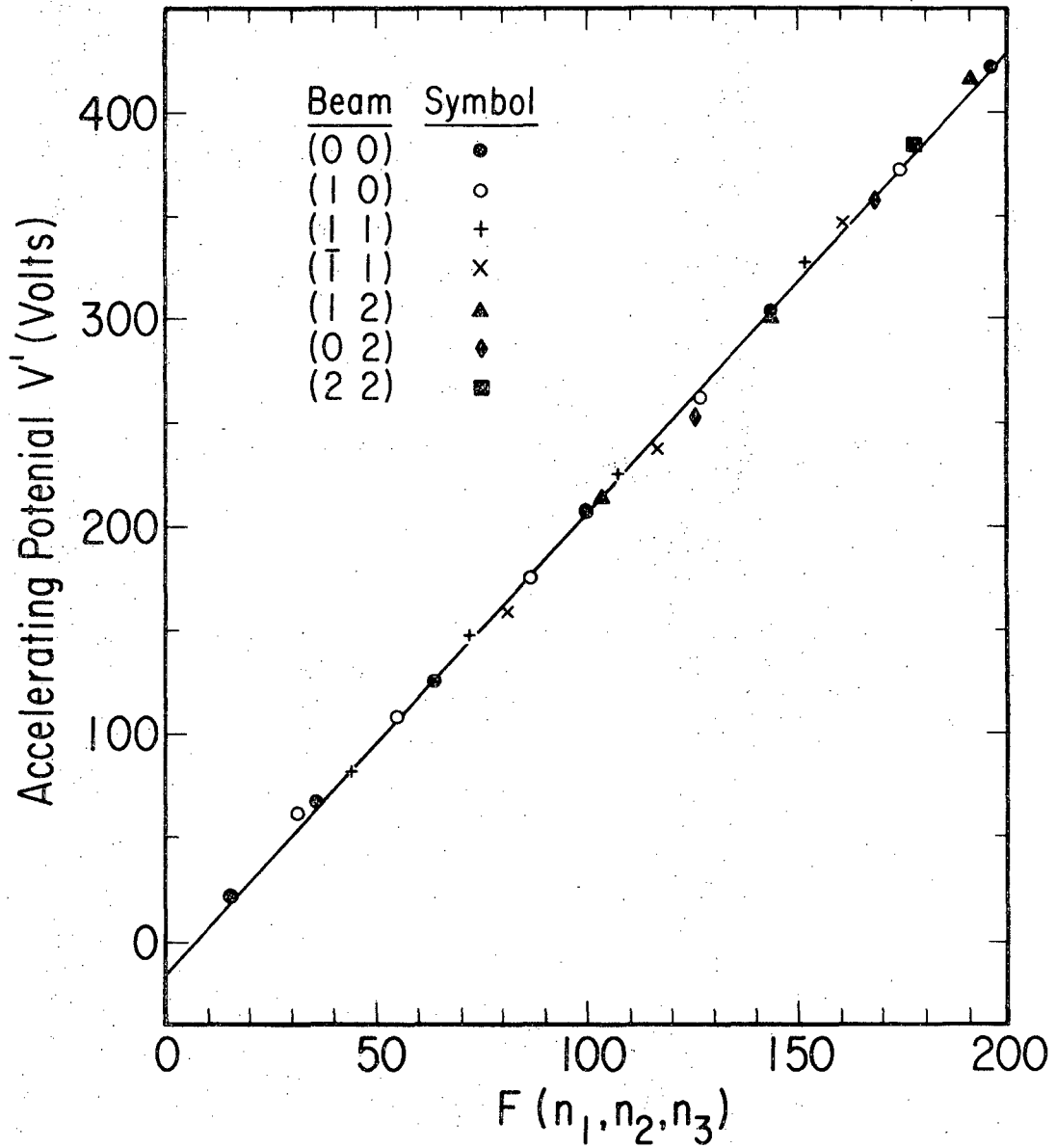
$(n_1 n_2 n_3)$	$F$	$V'_{\max}$	$(V_{\max} + V_0)$
002	8	22	20
003	18	68	64
004	32	126	126
005	50	207	206
006	72	304	304
007	98	421	419
102	15.7	62	54
103	27.6	108	107
104	43.5	176	177
105	63.5	262	266
106	87.4	372	372
113	22.3	82	83
114	36.1	148	144
115	54	226	224
116	76	328	321
$\bar{1}15$	40.5	159	164
$\bar{1}16$	58.5	237	244
$\bar{1}17$	80.2	347	341
125	52	215	215
126	72	302	304
127	95.5	416	408
026	63	253	263
027	84.5	358	359
226	89	384	379

comparison with  $V_{\max}(n_1, n_2, n_3)$ , calculated from Eq. (8) using the bulk values of  $a_0$ , 2.878 Å. The correctly indexed experimental results are entered in Table I. A plot of  $V'_{\max}(n_1, n_2, n_3)$  vs  $F(n_1, n_2, n_3)$  was then constructed, as shown in Fig. 10. The straight line is a least-squares fit to the points above 100 eV, and yields  $V_0 = -16.1$  eV. From the slope of  $4.44 = 37.6/a_0^2$ , the value  $a_0 = 2.91$  Å was determined. Finally,  $V_0$  and  $a_0$  obtained in this manner were used to calculate  $\{V_{\max}(n_1, n_2, n_3) + V_0\}$ . This quantity also appears in Table I, and is indicated by the arrows in the experimental intensity spectra, Figs. 8 and 9.

The preceding analysis shows that all of the strong observed intensity peaks are systematically accounted for by the model used. The inner potential determined in the analysis is in the range of those found for other metals, and the value of  $a_0$  is within 1% of the bulk value. Subsidiary structure in the intensity spectra was weaker by at least an order of magnitude, except at low energy, where multiple scattering is expected to be strong. Thus the single-scattering model appears to give a good account of the diffraction from the (110) surface of chromium.

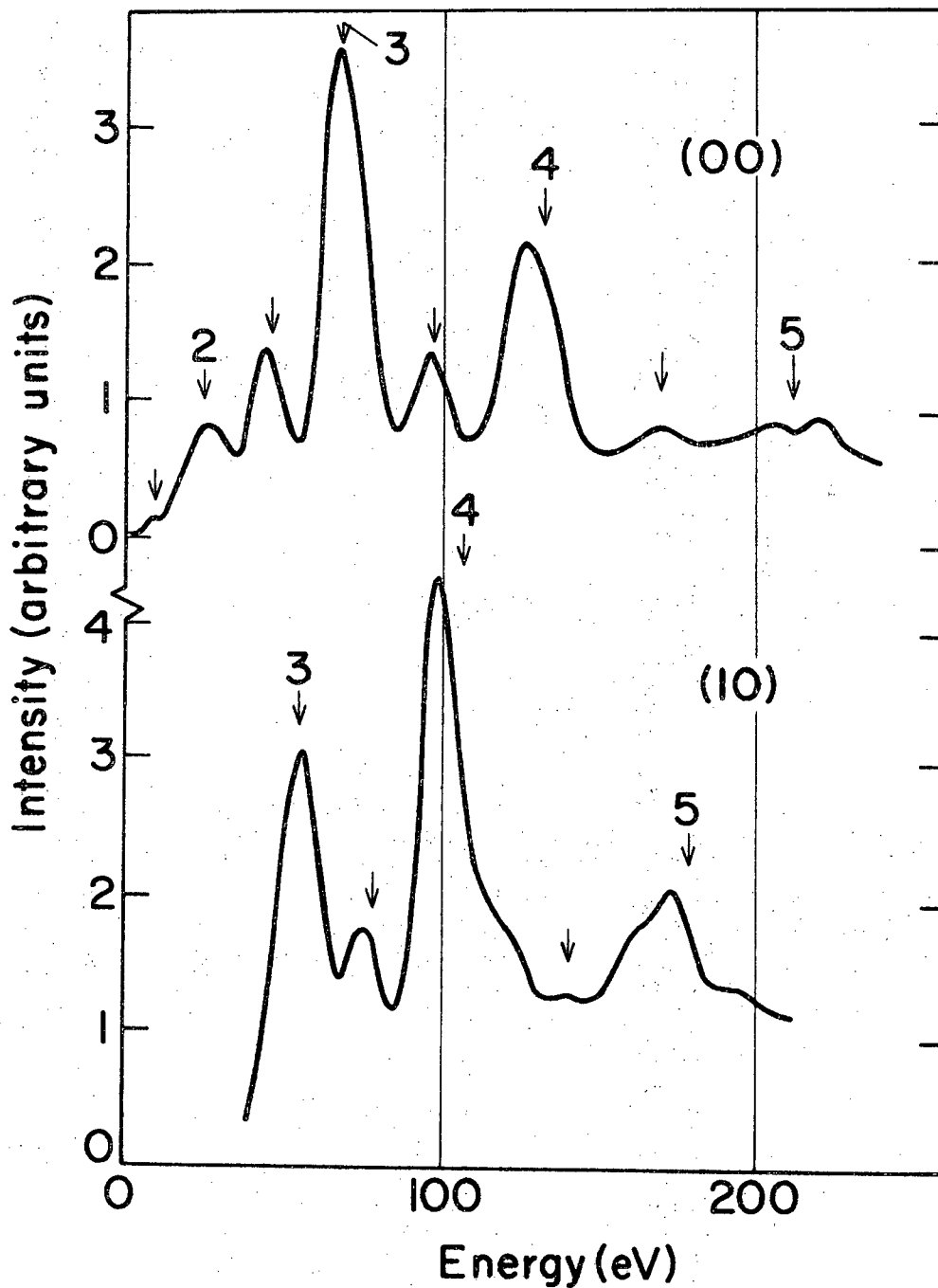
#### B. Al(100)

Intensity spectra for four diffraction beams from the aluminum (100) surface are shown in Figs. 11 and 12. These data<sup>5</sup> were obtained in a manner similar to that used in the work on chromium described earlier. Because aluminum has a much lower Debye characteristic temperature than chromium, the intensity spectra are not as easily obtained at high electron energies. Additionally, it is clear from Figs. 11 and 12 that the subsidiary intensity structure is relatively stronger than it is for chromium. It is believed that LEED in aluminum is dominated by multiple



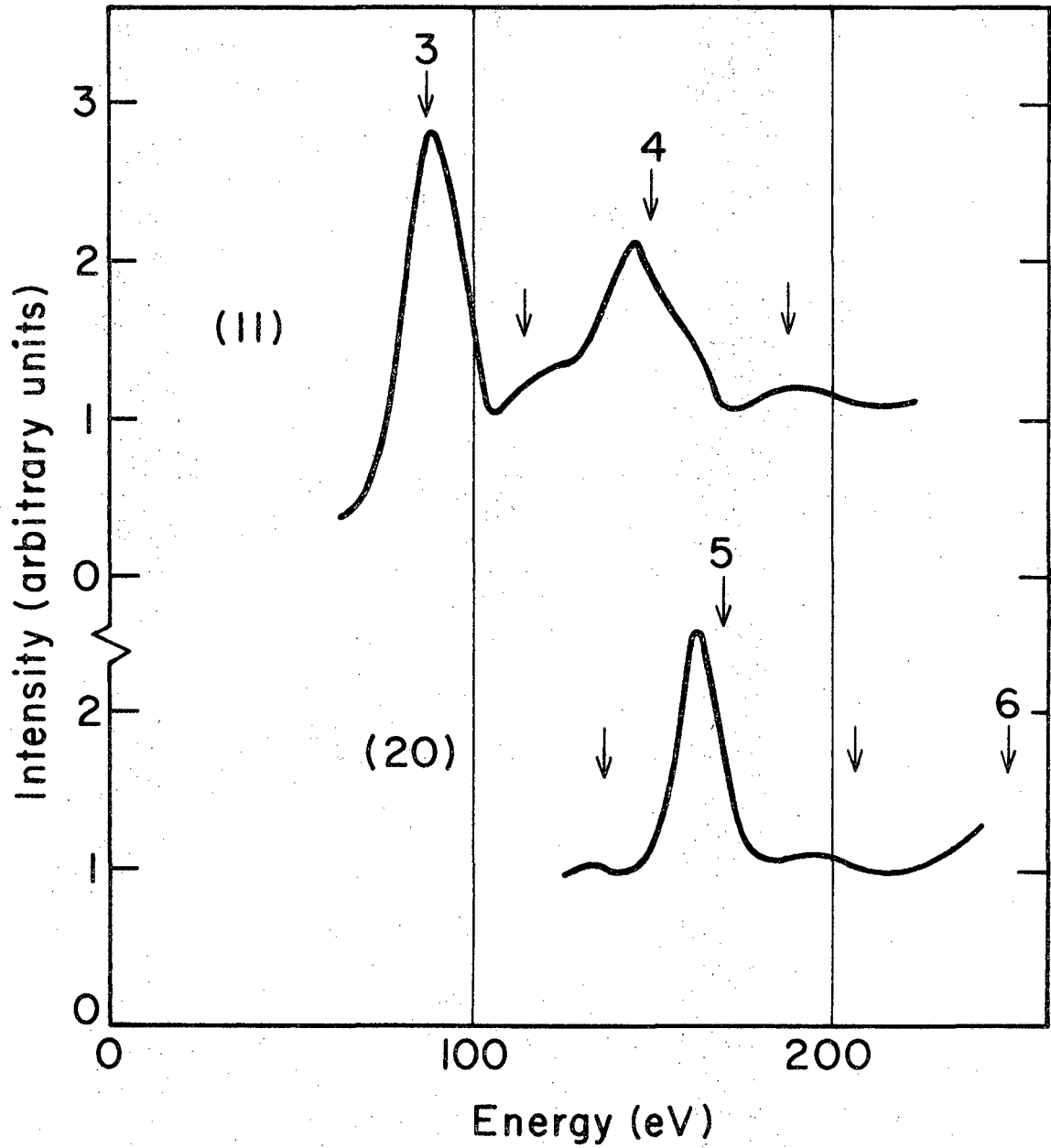
XBL 704-681

Fig. 10. Values of the accelerating potential at which intensity maxima were observed for the indicated diffraction beams, plotted vs corresponding values of  $F(n_1, n_2, n_3)$ , for the (110) surface of chromium.



XBL707-3460

Fig. 11. Intensity spectra for the (00) and (10) diffraction beams from the (100) surface of aluminum, obtained from Fig. 1 of Ref. 5. Numbered arrows indicate values of  $(V_{\max} + V_0)$  for integral order peaks, obtained in the analysis. Unnumbered arrows indicate the positions of the predicted half-integral order peaks.



XBL707-3462

Fig. 12. Intensity spectra for the (11) and (20) diffraction beams from the (100) surface of aluminum, obtained from Fig. 1 of Ref. 5. The arrows have the same significance as in Fig. 11.

scattering.<sup>6</sup> Nevertheless, it is instructive to attempt a kinematical analysis of the intensity data. For this purpose, in addition to Eq. (6), the following relations are required:

$$F(n_1, n_2, n_3) = \left\{ \frac{2n_1^2 + 2n_2^2 + (n_1 - n_2 + 2n_3)^2}{n_1 - n_2 + 2n_3} \right\}^2 \quad (10)$$

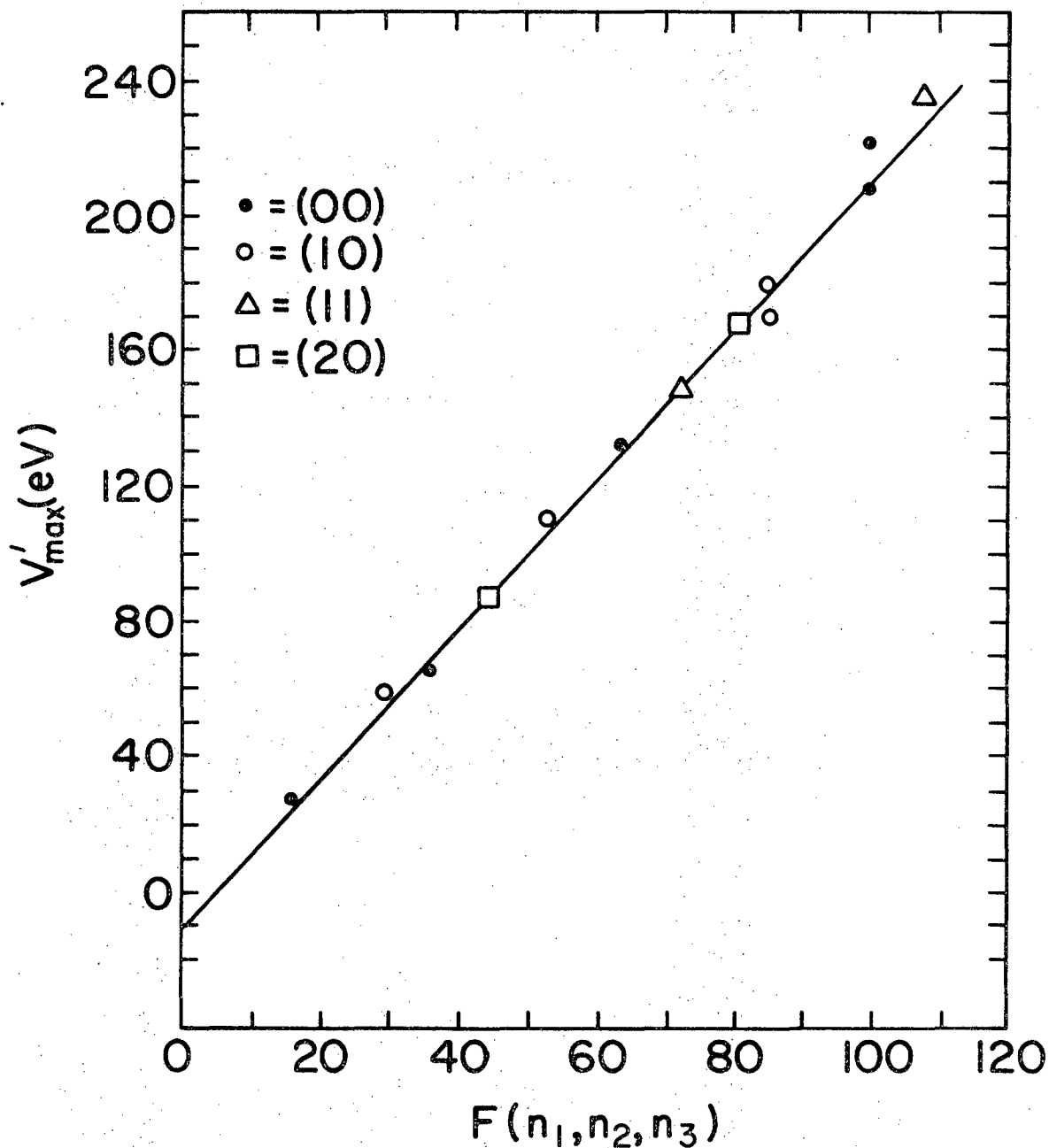
$$(00): \quad F = 4n_3^2,$$

$$(01): \quad F = \left\{ \frac{2 + (2n_3 - 1)^2}{2n_3 - 1} \right\}^2,$$

$$(11): \quad F = 4 \left\{ \frac{1 + n_3^2}{n_3} \right\}^2,$$

$$(02): \quad F = 4 \left\{ \frac{2 + (n_3 - 1)^2}{n_3 - 1} \right\}^2.$$

The analysis indicates that the prominent peaks in the intensity spectra occur at energies predicted by the single scattering model, with  $V_0 = 11$  eV and  $a_0 = 4.11$  A. (The bulk value of  $a_0$  is 4.04 A.) A plot of  $V_{\max}'(n_1, n_2, n_3)$  vs  $F(n_1, n_2, n_3)$  for these peaks is shown in Fig. 13. The remaining structure in the intensity spectra consists mainly of subsidiary maxima which alternate with the more prominent peaks. The extra structure may come from a variety of sources, among which is multiple scattering. A number of phenomena can lead to so-called "fractional-order" peaks predicted by kinematical theory. One explanation<sup>7</sup> of this occurrence, predicated on single scattering, invokes the fact that the scattering of slow electrons by atoms is peaked in the forward direction. Thus it may



XBL707-3459

Fig. 13. Values of the accelerating potential at which intensity maxima were observed<sup>5</sup> for the indicated diffraction beams, plotted vs corresponding values of  $F(n_1, n_2, n_3)$ , for the (100) surface of aluminum.

be necessary to consider phase relationships between electrons back-scattered from atoms that lie in rows parallel to the incident electron beam. In the case of normal incidence on an fcc(100) surface, atoms in alternate planes parallel to the surface meet this criterion. This should lead to the appearance of half-integral order peaks, whose positions may also be calculated using the preceding formalism. It is only necessary to redefine  $\vec{R}_1$ ,  $\vec{R}_2$ , and  $\vec{R}_3$ , and recalculate  $F(n_1, n_2, n_3)$ , for the case of an fcc crystal with alternate planes of atoms removed. The results obtained with

$$\vec{R}_1 = \frac{\sqrt{2}}{a_0} \begin{bmatrix} \hat{x} + \hat{y} \\ \sqrt{2} \end{bmatrix}, \quad \vec{R}_2 = \frac{\sqrt{2}}{a_0} \begin{bmatrix} \hat{x} - \hat{y} \\ \sqrt{2} \end{bmatrix}, \quad \vec{R}_3 = \frac{1}{a_0} [\hat{z}],$$

$$F(n_1, n_2, n_3') = \left\{ \frac{2n_1^2 + 2n_2^2 + n_3'^2}{n_3'} \right\}^2,$$

taking  $a_0 = 4.11 \text{ \AA}$  and  $V_0 = -11 \text{ eV}$ , are listed in Table II. Experimental results<sup>5</sup> for  $V'_{\max}$  are included for comparison. Alternate values of the tabulated quantities coincide with the integer order values determined previously, and plotted in Fig. 13. Additionally, half-integer order maxima are predicted. The latter are indicated by unnumbered arrows in Figs. 11 and 12. Their agreement with the observed intensity maxima, while reasonable, is not uniformly as good as that for the integer order case.

Thus the single scattering model appears to account satisfactorily for the positions of the prominent intensity maxima, for diffraction at normal incidence from the (100) surface of aluminum. Most of the remaining intensity structure appears to be reasonably well described by

Table II. Values of  $F$ ,  $V'_{\max}$ , and  $(V_{\max} + V_0)$  for the intensity maxima in LEED studies of the (100) surface of aluminum. The symbol \* identifies integral order maxima; the others are half-integral order. Energies are in eV.

$(n_1 n_2 n_3)$	$F$	$V'_{\max}$	$(V_{\max} + V_0)$
003	9	10	9
004*	16	27	25
005	25	48	45
006*	36	66	69
007	49	96	98
008*	64	128	132
009	81	169	170
0010*	100	208, 221	212
015*	29.2	59	54
016	40.1	72	78
017*	53.1	110	107
018	68	135	141
019*	85	170, 180	179
115	33.6	60	64
116*	44.4	88	88
117	57.2	118	116
118*	72.3	150	150
119	89.4	190	188
1110*	108	237	229
027	66.5	130	137
028*	81	168	170
029	98	200	207
0210*	117	---	249

extending the calculation to include half-integer order maxima. Analysis of the angular dependence of the intensity spectra, not pursued in the present work, would be an essential part of detailed studies of the scattering from aluminum.

## VI. DISCUSSION

The method described and illustrated above, for the analysis of intensity data in LEED, appears to be a convenient one, especially whenever diffraction beams other than the specular reflection are studied. As mentioned earlier, the present calculation of the energy dependence of the diffracted intensity ignores a number of contributions other than the normal phase relationships among the scattered electrons. For example, a complete expression for the intensity due to single scattering would include several other energy dependent factors, such as the Debye-Waller and atomic scattering factors. These introduce a weak, slowly varying energy dependence whose effect is to distort and shift the intensity peaks slightly. Another interesting contribution comes from the anisotropy of the lattice constant near the surface, due to an outward relaxation of the outermost atom layers. In general, it is felt that these contributions are too small to affect the data observably, unless special pains are taken to detect them.

Although the use of a purely kinematic model must always be questioned, it nevertheless provides a means of organizing the data in situations such as those encountered for chromium and aluminum. Furthermore, it has been suggested<sup>6</sup> that multiple scattering can lead to a distribution of intensity at energies predicted by a kinematic model, in which case the latter may be used in structural analysis studies. This is certainly a welcome prospect, in view of the great complexity of detailed multiple scattering calculations.

ACKNOWLEDGMENTS

The author is grateful to L. A. West and Professor G. A. Somorjai for their critical reading of this manuscript.

This work was done under the auspices of the U. S. Atomic Energy Commission.

REFERENCES

1. R. Kaplan and G. A. Somorjai, Observation of Zero-Point Atomic Motion Near the Cr(110) Surface by Low-Temperature Diffraction of Slow Electrons, UCRL-19664, July 1970 (to be published).
2. J. J. Lander in Advances in Solid State Chemistry, Van Nostrand Co., Inc., Princeton, N. J. (1957).
3. H. H. Farrell and G. A. Somorjai, in Advances in Chemical Physics, J. Wiley and Sons, N. Y. (1970); to be published.
4. E. A. Wood, J. Appl. Phys. 35, 1306 (1964).
5. H. H. Farrell and G. A. Somorjai, Phys. Rev. 182, 751 (1969).
6. C. W. Tucker, Jr. and C. B. Duke, "Synopsis of Predictions of the S-Wave Multiple Scattering Model With Damping," paper presented at the Fourth LEED Theory Seminar, Gaithersburg, Md., 1970.
7. R. L. Gerlach and T. N. Rhodin, Surf. Sci. 8, 1 (1967).

## LEGAL NOTICE

*This report was prepared as an account of Government sponsored work. Neither the United States, nor the Commission, nor any person acting on behalf of the Commission:*

- A. Makes any warranty or representation, expressed or implied, with respect to the accuracy, completeness, or usefulness of the information contained in this report, or that the use of any information, apparatus, method, or process disclosed in this report may not infringe privately owned rights; or*
- B. Assumes any liabilities with respect to the use of, or for damages resulting from the use of any information, apparatus, method, or process disclosed in this report.*

*As used in the above, "person acting on behalf of the Commission" includes any employee or contractor of the Commission, or employee of such contractor, to the extent that such employee or contractor of the Commission, or employee of such contractor prepares, disseminates, or provides access to, any information pursuant to his employment or contract with the Commission, or his employment with such contractor.*

TECHNICAL INFORMATION DIVISION  
LAWRENCE RADIATION LABORATORY  
UNIVERSITY OF CALIFORNIA  
BERKELEY, CALIFORNIA 94720